








Probing axion-like particles with multimessenger observations of neutron star mergers

Francesca Lecce ^{1,2,*} Alessandro Lella ^{1,2,†} Giuseppe Lucente ^{3,‡} Vimal Vijayan ^{4,§}
 Andreas Bauswein ^{4,¶} Maurizio Giannotti ^{5,6,**} and Alessandro Mirizzi ^{1,2,††}

¹*Dipartimento Interateneo di Fisica “Michelangelo Merlin”, Via Amendola 173, 70126 Bari, Italy*

²*Istituto Nazionale di Fisica Nucleare - Sezione di Bari, Via Orabona 4, 70126 Bari, Italy*

³*SLAC National Accelerator Laboratory, 2575 Sand Hill Rd, Menlo Park, CA 94025*

⁴*GSI Helmholtzzentrum für Schwerionenforschung, Planckstraße 1, 64291 Darmstadt, Germany*

⁵*Centro de Astropartículas y Física de Altas Energías,
 University of Zaragoza, Zaragoza, 50009, Aragón, Spain*

⁶*Physical Sciences, Barry University, 11300 NE 2nd Ave., Miami Shores, FL 33161, USA*

(Dated: July 3, 2025)

Axion-like particles (ALPs) can be copiously produced in binary neutron star (BNS) mergers through nucleon-nucleon bremsstrahlung if the ALP-nucleon couplings g_{aN} are sizable. The ALP-photon coupling $g_{a\gamma}$ may trigger conversions of ultralight ALPs into photons in the magnetic fields of the merger remnant and of the Milky Way. This effect would lead to a potentially observable short gamma-ray signal, in coincidence with the gravitational-wave signal produced during the merging process. This event could be detected through multi-messenger observation of BNS mergers employing the synergy between gravitational-wave detectors and gamma-ray telescopes. Here, we study the sensitivity of current and proposed MeV gamma-ray experiments to detect such a signal. As an explicit example, we consider ALP couplings related as in the Kim–Shifman–Vainshtein–Zakharov (KSVZ) axion model, and show that in this case the proposed instruments can reach a sensitivity down to $g_{a\gamma} \gtrsim \text{few} \times 10^{-13} \text{ GeV}^{-1}$ for $m_a \lesssim 10^{-9} \text{ eV}$, comparable with the SN 1987A limit.

I. INTRODUCTION

Axion-like particles (ALPs) are predicted in several extensions of the Standard Model (SM) of particle physics [1–6]. In particular, string theory can account for an “axiverse” with the QCD axion [7–10] and several ultralight ALPs [11–13]. Stellar environments represent ideal engines to produce ALPs, via their interactions with SM particles. Typically, one expects that ALPs are produced by (quasi-)thermal processes, so that the stellar ALP spectrum would show typical energies set by the temperature of the stellar plasma (see Ref. [14] for a review of different stellar axion fluxes). Remarkably, core-collapse supernovae (SNe), reaching a core temperature $T \sim 30 \text{ MeV}$, are the most energetic sources of stellar ALPs. Their production from the hot and dense nuclear medium in the SN core can be copious if ALPs would be coupled to nucleons [15–21]. The ALP-nucleon interactions are commonly described by the following Lagrangian [3]:

$$\mathcal{L}_{aN} = \frac{\partial_\mu a}{2m_N} \sum_{N=p,n} g_{aN} \bar{N} \gamma^\mu \gamma_5 N, \quad (1)$$

where a is the ALP field, m_N is the nucleon mass, and g_{aN} is the ALP coupling to nucleon species, with $N = p, n$ for protons and neutrons, respectively. This Lagrangian allows for ALP production via nucleon-nucleon (NN) bremsstrahlung [19]. An enhancement in ALP emissivity can be achieved if a significant fraction of thermal pions is present in the SN core, allowing for ALP production via pionic Compton-like (πN) processes [22]. In such a situation, SN 1987A neutrino observations would exclude values of $g_{aN} \gtrsim 10^{-9}$ in order to avoid a significant shortening of the neutrino burst [21].

Furthermore, one can consider scenarios in which ALPs are also coupled to photons through the following Lagrangian [23, 24]:

$$\mathcal{L}_{a\gamma} = -\frac{1}{4} g_{a\gamma} a F_{\mu\nu} \tilde{F}^{\mu\nu} = g_{a\gamma} a \mathbf{E} \cdot \mathbf{B}, \quad (2)$$

* francesca.lecce@ba.infn.it

† alessandro.lella@ba.infn.it

‡ giuseppe.lucente@ba.infn.it

§ v.vijayan@gsi.de

¶ a.bauswein@gsi.de

** mgiannotti@unizar.es

†† alessandro.mirizzi@ba.infn.it

where $g_{a\gamma}$ is the ALP-photon coupling, $F_{\mu\nu}$ is the electromagnetic field, and $\tilde{F}_{\mu\nu} = \frac{1}{2}\epsilon_{\mu\nu\rho\sigma}F^{\rho\sigma}$ is its dual. In the presence of the ALP-photon coupling, ultralight ALPs produced thanks to the ALP-nucleon coupling in Galactic SNe ($m_a \lesssim 10^{-10}$ eV) would efficiently convert within the Milky Way magnetic field, giving rise to a gamma-ray signal observable by gamma-ray experiments operating in the MeV energy range. The search of gamma-rays induced by ALPs from SNe would benefit from the simultaneous detection of SN neutrinos, which could serve as an external time trigger, linking the ALP signal to a specific supernova event.

This connection has been pointed out since the SN 1987A explosion [25–29]. At that time, the non-observation of the ALP-induced gamma-ray signal in the Gamma-Ray Spectrometer (GRS) of the Solar Maximum Mission (SMM) in coincidence with the neutrino signal from SN 1987A provided strong bounds on ALPs from SNe [30–34]. Recently, it has been shown that previous bounds can be strengthened significantly if one also accounts for ALP-photon conversions in the magnetic field of the progenitor star [35].

Binary neutron star (BNS) merger events represent an environment with similar physical properties with respect to SNe. Therefore, *mutatis mutandis*, one expects ALP production in the merger remnant by ALP-nucleon coupling (see Ref. [36] for merger simulations considering the effects of ALP bremsstrahlung) and conversions in gamma-rays in the magnetic field of the Milky Way as well as of the BNS remnant itself, thanks to the ALP-photon coupling. The NN bremsstrahlung process was considered in Ref. [37] as a production process for ALPs in BNS mergers. However, corrections beyond the one-pion-exchange approximation [19] were not included in that paper. Therefore, the authors obtained an overproduction of ALPs with respect to the correct calculation (see, e.g., Refs. [19–21] for the SN case). Furthermore, the ALP production from BNS mergers was also estimated in the recent Ref. [35]. However, in that work, the authors adopted an SN model, rather than a self-consistent model for the BNS merger event, to get a rough estimation of the ALP production from mergers. It is apparent that, at the moment, the characterization of ALP-induced signals from BNS mergers has not been carried at the same level of sophistication as in SNe. We devote this current work to fill this gap.

Unlike the case of SNe, BNS mergers are likely extra-galactic events. This prevents the possibility of using the neutrino signal as an external trigger for the ALP-induced gamma-ray burst with current detectors, as is possible in the case of Galactic SNe. However, for BNS merger events, one expects to detect a gravitational-wave (GW) signal with current detectors like LIGO [38] and VIRGO [39]; see, e.g., the recent multi-messenger observation of the BNS merger event GW170817 [40–43].

Due to the simultaneity of the ALP-induced gamma-ray burst and the GW signal, one would replace the neutrinos with a GW detection as an external trigger to determine the time at which one has to search for the ALP-induced gamma-ray signal in a gamma-ray telescope. Therefore, the possible multi-messenger detection of BNS merger events with GW interferometers plus gamma-ray telescopes widens the search for ALP-induced signals to an extragalactic horizon. We remark that in the case of the multi-messenger observation of the BNS merger GW 170817, *Fermi*-LAT was entering the South Atlantic Anomaly at the time of the LIGO/Virgo trigger and therefore cannot place constraints on the existence of a gamma-ray burst emission associated with the moment of binary coalescence [41]. However, a gamma-ray burst peaked at energies $E \sim 270$ keV was observed by the *Fermi* Gamma-ray Burst Monitor [40] with a delay of 1.7 s with respect to the GW trigger. Based on this observation, we assume that the standard gamma-ray burst expected after the merging can be distinguished from the ALP-induced signal due to this time delay. This expectation needs further investigations when better theoretical modeling of gamma-ray bursts from BNS mergers are available. Furthermore, it is not clear if every BNS merger produces a beamed relativistic outflow. At any rate, one would not expect a gamma-ray burst signal for the majority of merger events observed from equatorial directions.

In the following we discuss this proposal in detail. In Sec. II we present the BNS merger model used in our work. Then, in Sec. III we calculate the ALP energy spectrum from NN bremsstrahlung. In Sec. IV we characterize the ALP-photon conversions in the BNS remnant and in Milky Way magnetic fields. In Sec. V we briefly describe the gamma-ray telescopes we use in our analysis and present their sensitivity to the ALP-photon coupling $g_{a\gamma}$. Finally, in Sec. VI we discuss our results and conclude.

II. BNS MERGER MODEL

The merging of compact objects is a complex dynamical process, which requires expensive numerical simulations involving three-dimensional relativistic (magneto-)hydrodynamics, neutrino transport, and a model for the hot nuclear equation of state (see, e.g., Ref. [44]). These simulations show that during the post-merger evolution densities of a few times the nuclear saturation density and temperatures of several tens of MeV occur in the merger remnant. The merging is an inherently three-dimensional process with a distinguished axis defined by the orbital angular momentum of the binary. The post-merger remnant evolves into an approximately axi-symmetric object, which, due to the large amount of angular momentum, is strongly deformed. As an initial assessment, we consider radially-averaged properties of the merger remnant, which simplify the analysis while still providing transparent and reasonably accurate physical

insights.

For the present analysis, we adopt data from a simulation of a $1.375\text{-}1.375\ M_\odot$ BNS merger simulation using the DD2 equation of state [45]. The calculation was conducted with a three-dimensional relativistic smooth particle hydrodynamics code, which includes a neutrino treatment to model energy losses by neutrinos and neutrino reabsorption [46, 47]. The simulation covers the post-merger evolution until about 23 ms after merging.

The properties of the characteristic environment produced in the merger are shown in Fig. 1, where we display the radial temperature profile T (upper left panel) and the matter density ρ profile (upper right panel) at different times after merging. The quantities are averaged over polar and azimuthal angles. For $r \lesssim 5$ km, the temperature declines from ~ 25 MeV at $t = 5$ ms to ~ 15 MeV at $t = 15 - 20$ ms. At larger distances, the T profile is similar for the different post-merging times considered, and monotonically drops from $T \sim 15$ MeV at $r \sim 10$ km to a few MeV at $r \gtrsim 50$ km. The matter density ρ increases with time for $r \lesssim 5$ km, with a maximum in the center from $\rho \sim 6 \times 10^{14}$ g/cm³ at $t = 5$ ms to 7×10^{14} g/cm³ at $t = 20$ ms. At larger distances, the density shows a sharp drop around $r \sim 10$ km, marking the radius of the remnant of the BNS merger.

A. Nuclear matter effects

In presence of ALP-nucleon Lagrangian in Eq. (1), ALPs can be produced in BNS mergers by NN bremsstrahlung, involving protons and neutrons as relevant targets (see Sec. III). To accurately evaluate the ALP production rate, it is crucial to account for key aspects of the nuclear matter present in the BNS merger. In particular, the very high density reached in these environments, which exceeds nuclear saturation, requires a careful treatment of nucleon properties, as standard descriptions may no longer be valid. The combination of high density and relatively low temperature results in significant degeneracy effects, which cannot be neglected when modeling the nucleon population. Additionally, finite-density effects modify the bare nucleon mass, further influencing their role in ALP production. Accounting for these effects, the nucleon distribution can be written as

$$f_N = \frac{1}{1 + \exp[(E_N^{\text{kin}}(p, m_N^*) - \mu_N^*)/T]}, \quad (3)$$

where the kinetic energy is given by the modified dispersion relation [48–50]

$$E_N^{\text{kin}} = \sqrt{p^2 + m_N^{*2}}, \quad (4)$$

where p is the nucleon momentum and m_N^* denotes the *nucleon effective mass* [18]. This latter is defined as

$$m_N^* = m_N + \Sigma_S, \quad (5)$$

where Σ_S is the nucleon scalar self-energy and $m_p = 938$ MeV ($m_n = 939$ MeV) is the bare mass of the proton (neutron). In Fig. 1 we show the radial evolution of m_p^* (middle left panel) and m_n^* (bottom left panel). For $r \lesssim 5$ km, the effective masses of both species can be reduced down to ~ 300 MeV.

It is convenient to also consider the nucleon degeneracy parameters η_N , defined as [49]

$$\eta_N = \frac{\mu_N - m_N - U}{T}, \quad (6)$$

where μ_N is the nucleon chemical potential and $U = \Sigma_S + \Sigma_V$ the non relativistic mean-field potential of nucleons, with Σ_V being the nucleon vector self-energy and $\mu_N^* = \mu_N - U$ the so-called effective or kinetic chemical potential [49]. In particular, nucleons can be considered essentially degenerate for $\eta_N \gtrsim 1$ and non-degenerate for $\eta_N < 0$. Fig. 1 displays the radial evolution of η_p (middle right panel) and η_n (bottom right panel) at different times after merging. One realizes that protons are degenerate for $r \lesssim 6$ km and the transition to a non-degenerate state occurs at $r \gtrsim 6$ km. Additionally, the degeneracy parameter decreases more rapidly as time increases and presents a sharp drop at $r \sim 15$ km. On the other hand, neutrons show a significantly higher degeneracy parameter than protons in the inner regions of the remnant, so that they can be considered degenerate until $r \lesssim 10$ km as the transition to a non-degenerate state occurs at $r \gtrsim 10$ km.

III. ALP PRODUCTION IN BNS MERGER REMNANT

The ALP production via the ALP-nucleon Lagrangian of Eq. (1) has been widely studied in the context of SNe, where NN bremsstrahlung $N + N \rightarrow N + N + a$ [15–19] and pionic Compton processes $\pi + N \rightarrow N + a$ [17, 22, 51]

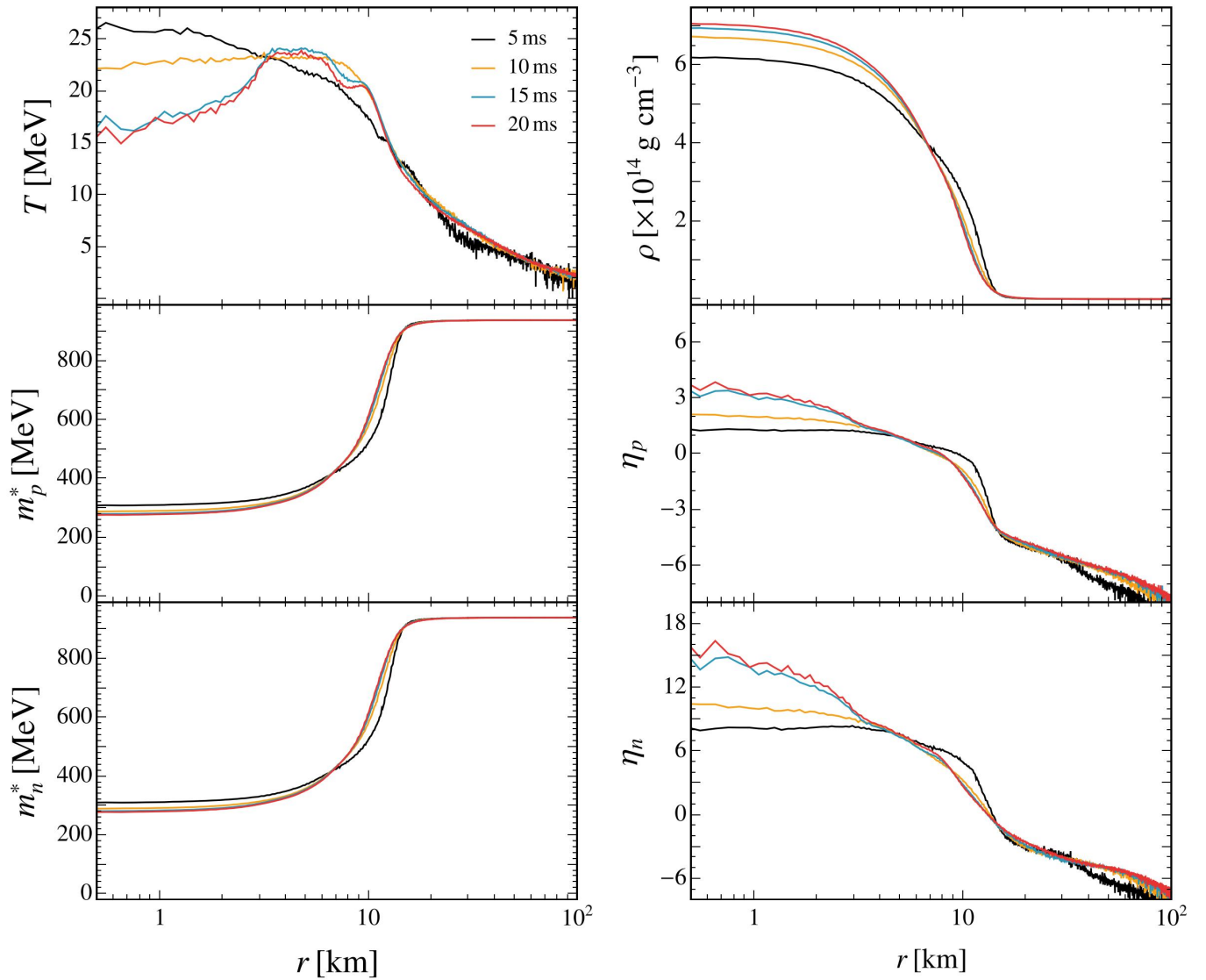


FIG. 1. Radial evolution at different post-merging times for different quantities from the adopted BNS merger model. *Left panels:* From top to bottom, temperature T , effective proton mass m_p^* and effective neutron mass m_n^* . *Right panels:* From top to bottom, density ρ , proton degeneracy factor η_p and neutron degeneracy factor η_n .

have been considered. In particular, recent NN bremsstrahlung calculations have introduced corrections to the naive one-pion-exchange approximation. Notably, these include many-body effects on the nucleon dispersion relations in the medium and its finite lifetime due to multiple scattering [19] (see also Ref. [52] for a recent work on a self-consistent approach for ALP production in dense environments). Furthermore, in the presence of a significant fraction of thermal pions, it has been shown that pionic processes may significantly increase the ALP emissivity, as shown in Ref. [20]. We refer to this latter paper for the state-of-the-art calculation of the SN emissivities for these processes.

In the following, we apply the results of these previous works to evaluate the ALP emissivity from BNS due to the ALP-nucleon coupling g_{aN} . In particular, we focus on the NN bremsstrahlung process only, neglecting the pionic process. This choice is motivated by the very high densities reached during the merging event, which may lead to the bosonic condensation of pions in vast regions of the environment under study with only a smaller contribution of thermal pions [53, 54]. The role of pions in ALP production deserves a dedicated study, which we postpone to a future work. Moreover, under these assumptions, our results should be considered as conservative.

Effects due to the strong gravitational field in the BNS, such as time dilation and energy redshift, significantly impact the ALP emission. Here, these effects have been incorporated into the ALP spectrum by introducing the lapse factor $\alpha_{\text{GR}}(r) \leq 1$ (see Refs. [20, 55]). The lapse factor modifies energy and time as follows:

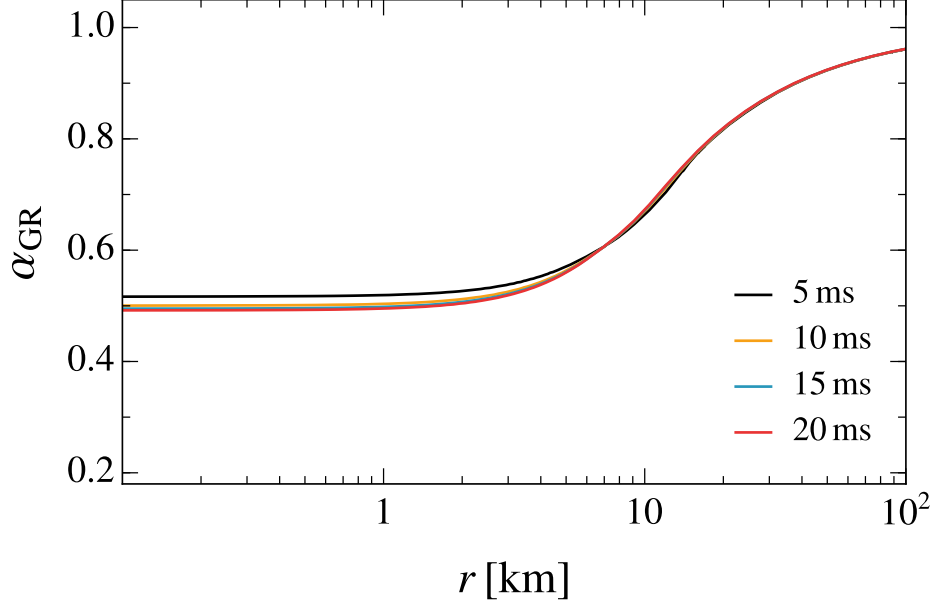


FIG. 2. Radial evolution at different post-merging times of the lapse factor $\alpha_{\text{GR}}(r)$.

$$\begin{aligned} E &= E^*(r) \alpha_{\text{GR}}(r), \\ dt &= dt^*(r) \alpha_{\text{GR}}^{-1}(r), \end{aligned} \quad (7)$$

where $E^*(r)$ and $dt^*(r)$ are the local energy and time interval, while E and dt are the same quantities as observed at infinity. The relations in Eq. (7) imply that

$$dE^* dt^* = dE dt. \quad (8)$$

In Fig. 2 we show the evolution of the radial profile of $\alpha_{\text{GR}}(r)$ for different times after merging. We see that $\alpha_{\text{GR}} \sim 0.5$ for $r \lesssim 10$ km, while it approaches 1 at $r \gtrsim 100$ km.

Given the above considerations, starting from the expressions for the ALP production spectrum per unit volume $d^2 n_a / dE_a dt$ introduced in Ref. [20], the red-shifted ALP spectrum is obtained by integrating over the volume of the merger remnant using the angle averaged profiles and time,

$$\frac{dN}{dE} = \int dV dt \frac{d^2 n_a}{dt dE} = \int dV dt^* \frac{d^2 n_a}{dt^* dE^*} \alpha_{\text{GR}}^{-1}(r). \quad (9)$$

In the time integration, we assume that the input quantities of the BNS models remain constant from 20 ms up to 1 s after merging, as done in previous ALP studies [56, 57]. This approach may somewhat overestimate the strength of the signal because the cooling time scale of the merger remnant is of order 1 s and the merger remnant may collapse to a black hole, which would significantly reduce the production of ALPs.

The resulting time-integrated spectrum is shown in Fig. 3 (solid curve), where we set $g_{ap} = 10^{-10}$ and $g_{an} = 0$. Since $m_a \ll T$, the ALP spectrum can be approximated with excellent precision using the following analytical expression [32]:

$$\frac{dN}{dE} = C \left(\frac{g_{ap}}{10^{-10}} \right)^2 \left(\frac{E}{E_0} \right)^\beta \exp \left(-\frac{(\beta+1)E}{E_0} \right), \quad (10)$$

where we obtain $C = 1.57 \times 10^{52} \text{ MeV}^{-1}$, $E_0 = 36.9 \text{ MeV}$, and $\beta = 1.3$. For comparison, in Fig. 3 we show as a black dashed curve the SN ALP spectrum obtained by setting $g_{ap} \sim 10^{-10}$ and $g_{an} = 0$, in analogy with the BNS case. We highlight that for SN emission the spectrum presents two peaks: the first at $E \sim 50$ MeV associated with the NN process, and the second at $E \sim 150$ MeV due to the πN production. Comparing the ALP spectrum from BNS mergers with that from SNe, we realize that the first one is peaked at lower energies $E \sim 30$ MeV and it is suppressed by ~ 2 orders of magnitude with respect to the SN one for the same ALP-nucleon couplings. This trend

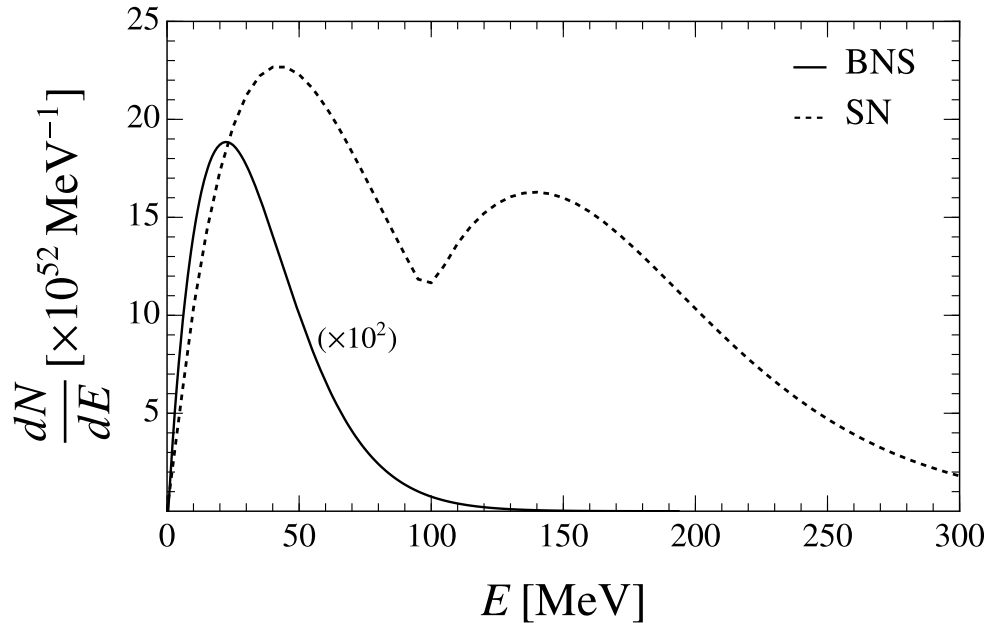


FIG. 3. Time-integrated ALP emission spectrum by means of NN bremsstrahlung from the BNS (solid curve) and from SN (dashed curve). Here we set $g_{ap} = 10^{-10}$ and $g_{an} = 0$. Note that in the case of the SN the pionic processes are included.

can be related to the lower temperature of BNS matter compared to that in the SN core. In addition, the stronger degeneracy of the nucleon population leads to a further reduction of the emission rates. Finally, ALP emission from BNS mergers has been assumed to occur on a time scale of $\lesssim 1$ s, shorter than the ~ 10 s emission from SNe. All of these effects go in the same direction, resulting in a suppression of the ALP emission rate in BNS mergers with respect to the SN case. Although assuming two identical neutron stars in the merging process typically enhances the temperature of the profile [57], we note that averaging the thermodynamic properties of the merger remnant may lead to an underestimation of the emission because of the non-linear temperature dependence. Averaged out, high-temperature regions may affect the emissivity more significantly. We also remark that the average temperature of the merger remnant approximately increases with the softness of the EoS [58] (see Fig. 18 therein), while we adopted the rather stiff DD2 EoS [45] in our merger model.

In the following, when accounting for both ALP-nucleon and ALP-photon couplings, we consider an exemplary scenario inspired by the Kim-Shifman-Vainshtein-Zakharov (KSVZ) axion model [59, 60]. In this case, the ALP couplings to photons and protons can be related as follows:

$$g_{ap} = \frac{2\pi m_N}{\alpha} \frac{C_{ap}}{C_{a\gamma}} g_{a\gamma}, \quad (11)$$

where α is the electromagnetic fine-structure constant, and $C_{ap} \simeq -0.47$ and $C_{a\gamma} \simeq -1.92$ are model dependent constants set by the UV completion of the model [61]. Here, we remark that $g_{an} \simeq 0$ in the canonical KSVZ axion model. For the couplings of this model, the bremsstrahlung production rate is always dominant over the Primakoff one associated with $g_{a\gamma}$, so we will neglect this latter hereafter. We also stress that for axion-nucleon couplings below the SN 1987A bound, i.e., $g_{aN} \lesssim 10^{-9}$, it was shown in Ref. [62] that ALPs would be in a free-streaming regime, so we can safely neglect reabsorption in the nuclear medium inside the dense BNS merger environments.

IV. ALP-PHOTON CONVERSIONS IN MAGNETIC FIELDS

A. BNS magnetic field

After being emitted during the BNS merger event, ALPs travel long distances before reaching the observer located on the Earth. Notably, along their path from the emission site, ALPs can encounter regions hosting magnetic fields around the remnant, within the host-galaxy, in the intergalactic medium and the Milky Way. In particular, the post-merger remnant is expected to be surrounded by a strongly-magnetized medium. The evolution of the BNS merger

system is usually described by complex general-relativity magnetohydrodynamics simulations tracking the evolution of the BNS system from the pre- to post-merging phase (see Refs. [44, 63–65] for some recent reviews on the topic). Initial magnetic fields are significantly amplified during the merging and subsequent evolution of the differentially rotating merger remnant by various processes, such as the Kelvin-Helmholtz instability in the shear layer, magnetic winding, and the development of the magneto-rotational instability. Ultimately, magnetic fields in the remnant and its surroundings can even exceed 10^{15} G. For the sake of simplicity, in the following we assume that a few milliseconds after the merging the remnant B -field can be modeled through a dipolar magnetar-like structure,

$$B(r) = B_0 \left(\frac{r_0}{r} \right)^3, \quad (12)$$

where $r_0 = 10$ km is the remnant radius and we conservatively assume a surface magnetic field strength $B_0 = 10^{15}$ G.

For relativistic ALPs following radial trajectories, the conversions within the remnant magnetosphere of ALPs into photons can be tracked by employing a Schrödinger like equation of the form [24, 66, 67]

$$\left(i \frac{d}{dr} - E \right) \begin{pmatrix} \gamma_{\parallel}(r) \\ a(r) \end{pmatrix} = \begin{pmatrix} \Delta_{\text{HE}}^{\parallel}(r) & \Delta_{a\gamma} \\ \Delta_{a\gamma} & \Delta_a \end{pmatrix} \begin{pmatrix} \gamma_{\parallel}(r) \\ a(r) \end{pmatrix}, \quad (13)$$

where $\Delta_{\text{HE}}^{\parallel}$ is the QED vacuum polarization term in the Euler-Heisenberg limit [68], $\Delta_{a\gamma}$ is the ALP-photon mixing term, and Δ_a is the ALP mass term. We highlight that in this expression the ALP only mixes with the polarization of the photon field parallel to the projection of \mathbf{B} in the transverse plane with respect to the beam propagation direction \mathbf{B}_T . Moreover, in this context we have

$$\begin{aligned} \Delta_{\text{HE}}^{\parallel} &= \frac{7\alpha}{90\pi B_{\text{crit}}^2} E B_T^2 \simeq 4.7 \times 10^{15} \left(\frac{E}{10 \text{ MeV}} \right) \left(\frac{B_0}{10^{15} \text{ G}} \right)^2 \left(\frac{r}{r_0} \right)^{-6} \text{ km}^{-1}, \\ \Delta_{a\gamma} &= \frac{1}{2} g_{a\gamma} B_T \simeq 4.9 \times 10^3 \left(\frac{g_{a\gamma}}{10^{-11} \text{ GeV}^{-1}} \right) \left(\frac{B_0}{10^{15} \text{ G}} \right) \left(\frac{r}{r_0} \right)^{-3} \text{ km}^{-1}, \\ \Delta_a &= -\frac{m_a^2}{2E} \simeq 2.5 \times 10^{-6} \left(\frac{m_a}{10^{-4} \text{ eV}} \right)^2 \left(\frac{E}{10 \text{ MeV}} \right)^{-1}, \end{aligned} \quad (14)$$

with $B_{\text{crit}} = 4.41 \times 10^{13}$ G. For simplicity, in these expressions we neglect the angular dependence in the remnant magnetic field. From Eq. (14), it is apparent that ALP-photon conversions are strongly suppressed by QED vacuum effects close to the remnant surface. Conversely, we observe that conversion probabilities become sizable at $r \gtrsim 10^4 r_0$, where $\Delta_{\text{HE}}^{\parallel} \sim \Delta_{a\gamma}$ [66].

We plot the conversion probability $P_{a\gamma}$ in the BNS remnant field as the black curves in the left panels of Fig. 4, assuming $g_{a\gamma} = 10^{-12} \text{ GeV}^{-1}$. We realize that for $m_a \lesssim 10^{-7} \text{ eV}$, $P_{a\gamma}$ is in the range $10^{-7} - 10^{-9}$. Then, for ALP masses $m_a \gtrsim 10^{-4} \text{ eV}$, at the surface $r \simeq 10^4 r_0$ one finds $\Delta_a \gtrsim \Delta_{a\gamma}$. Thus, ALP-photon oscillations become incoherent and energy-dependent. Therefore, as shown in the lower left panel for $m_a = 10^{-3} \text{ eV}$, related conversion probabilities are strongly suppressed in this mass range.

B. Milky Way magnetic field

As they are extremely weakly interacting, the probability of ALPs escaping the remnant magnetosphere to interact with matter in the interstellar medium is negligible for all practical purposes. Furthermore, for the range of parameters we are interested in, the ALP lifetime

$$\tau_{a\gamma\gamma} = 1.32 \times 10^{25} \left(\frac{\text{eV}}{m_a} \right)^3 \left(\frac{10^{-10} \text{ GeV}^{-1}}{g_{a\gamma}} \right)^2 \text{ s} \quad (15)$$

is much larger than the age of the Universe. Moreover, as discussed in Sec. IV A, in the range of couplings $g_{a\gamma} < 10^{-10}$, only a negligible fraction of ALPs can be converted into photons in the remnant magnetosphere. Then, we are allowed to assume that the emitted ALP flux during the BNS merger remains unaffected when escaping the remnant volume and can encounter other large-scale astrophysical magnetic fields along its path.

Concerning the galaxy hosting the BNS merger event, one would expect B -fields characterized by the same strength of the Milky Way, i.e., $\mathcal{O}(1) \mu\text{G}$, on similar size of ~ 10 kpc [70–72]. As we will comment below, for such values conversion probabilities are expected to be $\mathcal{O}(10^{-4})$. Therefore, one does not expect a sizable depletion of the initial

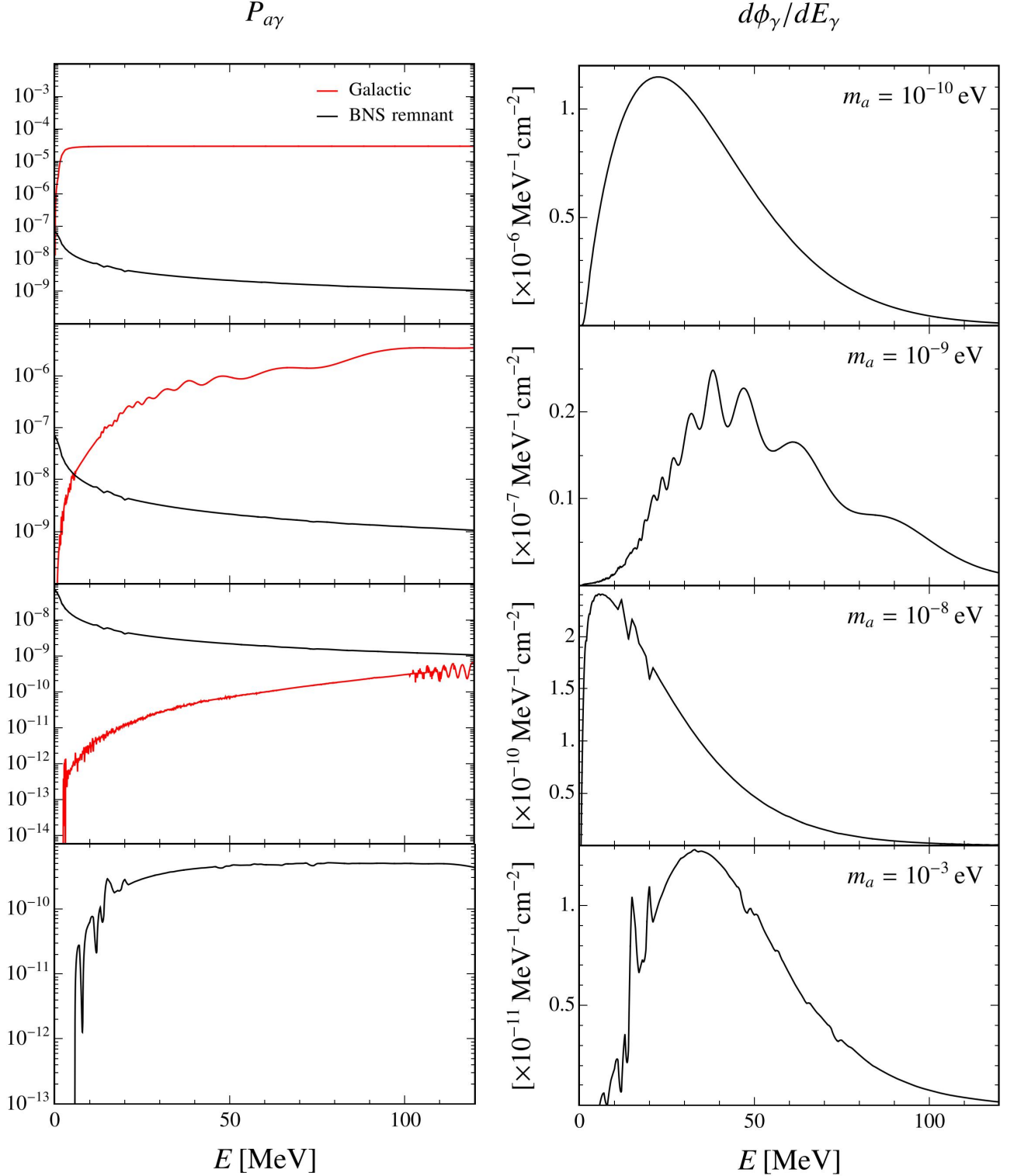


FIG. 4. *Left panels:* ALP-photon conversion probability as a function of the ALP energy for $g_{a\gamma} = 10^{-12} \text{ GeV}^{-1}$, in the BNS remnant field (black curves) and the Milky Way magnetic field. Conversions in the Milky Way are computed by modeling the Galactic magnetic field as in Ref. [69] and assuming an ALP beam propagating in the direction $(\ell, b) = (308.38^\circ, 39.30^\circ)$ (red curves). *Right panels:* Photon spectra induced by ALP-photon conversions in sequence in the BNS remnant magnetic field and the Galactic magnetic field. ALP emission is assumed to occur from a BNS event located at $d = 40 \text{ Mpc}$ from the observer on the Earth. From top to bottom the panels refer to ALPs with masses $m_a = 10^{-10}, 10^{-9}, 10^{-8}, 10^{-3} \text{ eV}$, respectively. Note that at $m_a \sim 10^{-3} \text{ eV}$ the conversion probability in the Milky Way magnetic field is negligible.

ALP flux due to this effect. Conversely, the produced photon flux by conversion in the host galaxy would be of the same level as that produced by conversions in the Milky Way. However, lacking detailed models of the magnetic fields, in order to avoid additional uncertainties we prefer to neglect ALP conversions in the host galaxies. This is a conservative choice that implies that we are neglecting a component of the gamma-ray flux produced by ALP conversions at the same level of the one produced in the Milky Way. Then, magnetic fields in intergalactic regions may play a significant role in ALP-photon conversions, depending on the parameters characterizing these fields [73, 74]. However, extragalactic magnetic fields are subject to very large uncertainties regarding their strength and typical correlation scales [75–77]. Therefore, in our estimation of the ALP conversion probability, we also conservatively neglect the contribution from magnetic fields outside the Milky Way.

On the other hand, the large-scale Galactic magnetic field can be well described by different models able to reproduce related gamma-ray observations [69, 78, 79]. In this work, we assume the Jansson-Farrar model [69] as a benchmark model for the Milky Way regular magnetic field, which takes into account a disk field and an extended halo field with an out-of-plane component, based on the WMAP7 Galactic synchrotron emission map [80] and extra-galactic Faraday rotation measurements. In particular, we employ the updated parameters given in Table C.2 of Ref. [81] (“Jansson12c” ordered fields), matching the polarized synchrotron and dust emission measured by the Planck satellite [82–84].

In general, the description of the ALP propagation throughout the Galactic magnetic field model requires a full three-dimensional approach. In this work, we closely follow the treatment outlined in Ref. [85] to numerically solve the dynamics of the coupled ALP-photon system along a given line of sight. As an exemplary scenario, in the following we consider the case of an ALP beam propagating from a generic source located at a distance $d = 40$ Mpc from the observer in the same sky location as the GW170817 event $(\ell, b) = (308.38^\circ, 39.30^\circ)$, where ℓ and b are the Galactic latitude and longitude, respectively [86]. Moreover, we trace ALP-photon conversions within the Milky Way magnetic field for $L = 20$ kpc, which is the typical size associated with the Galactic disk. The left panels of Fig. 4 depict in red the behavior of the ALP-to-photon conversion probability as a function of the ALP energy and for four representative ALP masses.

As discussed in Ref. [87], for ALP masses

$$m_a \ll 0.36 \text{ eV} \left(\frac{E_a}{100 \text{ MeV}} \right)^{1/2} \left(\frac{L}{10 \text{ kpc}} \right)^{-1/2}, \quad (16)$$

ALP-photon oscillations become energy-independent. In this regime, the conversion probability can be well approximated by

$$P_{a\gamma} \simeq 2.3 \times 10^{-4} \left(\frac{g_{a\gamma}}{10^{-12} \text{ GeV}^{-1}} \right)^2 \left(\frac{L}{10 \text{ kpc}} \right)^2 \left(\frac{B_T}{10^{-6} \text{ G}} \right)^2, \quad (17)$$

where B_T is the magnitude of the transverse component of the magnetic field averaged along the given line of sight [87]. In this regard, we point out that the Galactic ALP-photon conversion probability depends on the arbitrary choice of the line of sight along which the event is located. To evaluate the impact of this choice on the analysis, we estimate the value of the conversion probability by averaging over all of the possible lines of sight. We obtained that this procedure leads to a variation of less than a factor of 2 in the conversion probability. We can observe that for ALPs with mass $m_a = 10^{-10}$ eV the condition in Eq. (16) is always met in the energy range of interest for this study, and conversions in the BNS remnant are subleading with respect to those in the Milky Way. We point out the different trends of the conversion probability at low energies for the Galactic magnetic field compared to the source field. In particular, for $E \rightarrow 0$, the mass term, which dominates ALP-photon conversions in the Milky Way, is rapidly increased. Therefore, the Galactic conversion probability becomes energy dependent and gets suppressed. On the other hand, conversions in the remnant field are dominated by QED vacuum effects, which are washed at $E = 0$ [see Eq. (14)]. Thus, ALP-photon oscillations can take place in the inner region of the remnant magnetosphere where fields are stronger, resulting in a larger conversion probability.

In the coherent regime, the induced gamma-ray flux

$$\frac{d\phi_\gamma}{dE_\gamma}(E, L) = \frac{1}{4\pi d^2} \frac{dN}{dE}(E) P_{a\gamma}(E, L), \quad (18)$$

reproduces the same spectral shape of the ALP emission rate from the BNS event (see right panels of Fig. 3). On the other hand, the Galactic conversion probability for ALPs with masses $m_a = 10^{-9}$ eV starts to be suppressed in the energy range of interest, still remaining dominant with respect to the conversion probability in the remnant magnetic field. Thus, the related gamma-ray spectrum appears one order of magnitude smaller with respect to the previous case and shows a peculiar oscillatory behavior in the energy range $E \lesssim 100$ MeV. Finally, ALP-photon oscillations in the Galaxy become incoherent across the entire energy range considered for ALPs with masses $m_a > 10^{-9}$ eV. As a

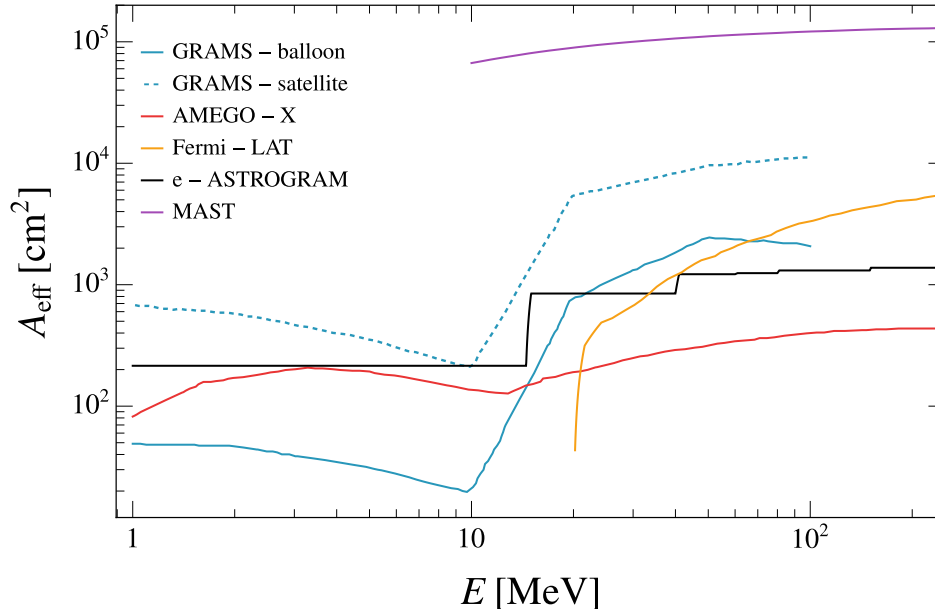


FIG. 5. Effective areas of e-ASTROGRAM [88], AMEGO-X [89], *Fermi*-LAT [90], GRAMS-balloon [91], GRAMS-satellite [91], and MAST [92] as functions of the energy of the incoming photon in the energy range relevant for this work.

result, for $m_a > 10^{-8}$ eV, conversions in the BNS remnant become the dominant contribution. Nevertheless, even when accounting for the magnetic field of the remnant, the gamma-ray flux associated with ALPs of mass m_a larger than a few neV is significantly suppressed.

V. SENSITIVITY OF GAMMA-RAY EXPERIMENTS TO ALPS FROM BNS MERGERS

A. Gamma-ray experiments

The detectability of the gamma-ray burst induced by conversions of ALPs emitted during BNS events is directly related to the properties of current and planned gamma-ray detectors operating in the 1–200 MeV energy ranges. Among the ones considered in this work, only *Fermi*-LAT is currently operational, while the others have been proposed for future missions. The main characteristics of these experiments are summarized in Fig. 5 and Table I. In particular, Fig. 5 displays the effective area of the different experiments in their operational energy ranges. This feature is crucial in determining whether the expected gamma-ray spectrum falls within the experiment’s sensitivity. We observe that proposed gamma-ray experiments such as e-ASTROGRAM [88] and AMEGO-X [89] would be able to cover the entire range of energies associated with ALP emission from BNS merger events. Conversely, *Fermi*-LAT [90] is subject to a dramatic loss of sensitivity at energies $E \lesssim 30$ MeV, where a significant fraction of the flux is expected. Similarly, both GRAMS-satellite and GRAMS-balloon [91] are limited to detecting photons up to 100 MeV, missing the high-energy tail of the spectrum. Therefore, the effects of the large effective areas of *Fermi*-LAT and GRAMS-satellite on the sensitivity is counterbalanced by the lack of coverage of the entire energy range of interest. It is worth noting that GRAMS-satellite offers an improvement in the effective area of approximately one order of magnitude compared to its balloon counterpart. Indeed, according to Ref. [91], the satellite version, which could be launched in the 2030s, will incorporate upgrades to the detector that are expected to significantly enhance the experiment’s sensitivity. Finally, MAST [92] exhibits a higher effective area for $E > 10$ MeV. However, since in Ref. [92] other specifics of the detector were defined only above 100 MeV, our analysis is conducted assuming this latter energy value as a threshold. From Tab. I, we observe that GRAMS-satellite and GRAMS-balloon feature a broad field of view, FoV = 6.3 sr, covering half of the sky for each single pointing. This significantly increases its probability of detecting an ALP-induced gamma-ray signal from a BNS merger event.

The number of background events N_{bkg} for each experiment is shown in Tab. I. For e-ASTROGRAM, this number is obtained by summing the background rate of all of the energy bins of interest provided in Tab. 4 of Ref. [88]. For all of the other experiments, the background events are estimated based on a background flux $d\phi_{\gamma,\text{bkg}}/dE$ expressed in

Experiment	FoV (sr)	$\delta\theta$ ($^\circ$)	N_{bkg} (counts s $^{-1}$)
e-ASTROGRAM [88]	$\gtrsim 2.5$	$\lesssim 1.5$	0.06
AMEGO-X [89]	2.5	3	0.25
<i>Fermi</i> -LAT [90]	2.4	$\lesssim 0.15$	0.08
GRAMS-balloon [91]	6.3	3	0.27
GRAMS-satellite [91]	6.3	1.8	0.35
MAST [92]	2.5	$\lesssim 1$	0.0004

TABLE I. Main features characterizing the current and future gamma-ray experiments considered in this work.

units of $\text{cm}^{-2} \text{s}^{-1} \text{MeV}^{-1} \text{sr}^{-1}$, assumed to be isotropic. Given the background flux, the effective area A_{eff} illustrated in Fig. 5, and the angular resolution of the considered experiment, the number of background events can be computed as

$$N_{\text{bkg}} = \Omega \times \int_{E_{\text{min}}}^{E_{\text{max}}} dE \frac{d\phi_{\gamma, \text{bkg}}}{dE} A_{\text{eff}}(E), \quad (19)$$

where

$$\Omega = 2\pi (1 - \cos \delta\theta), \quad (20)$$

is the solid angle corresponding to the angular resolution $\delta\theta$ (for $\delta\theta \ll 1$, $\Omega \sim 2\pi(\delta\theta)^2$), and E_{min} and E_{max} represent the lowest and highest energy values of the considered experiment. Specifically, the background events reported in the third column of Tab. I are obtained using information in Refs. [90, 93] for *Fermi*-LAT, Ref. [88] for e-ASTROGRAM, Refs. [89, 94] for AMEGO-X, Ref. [91] for GRAMS-satellite and GRAMS-balloon, and Ref. [92] for MAST. The specific energy ranges of interest in our study correspond to the energy coverage of the effective area shown in Fig. 5. Among the considered experiments, MAST exhibits the lowest number of background events (see Tab. I). Conversely, GRAMS-balloon and AMEGO-X, due to their poor angular resolution, yield a higher number of background events. Finally, GRAMS-satellite records the highest number of background events, surpassing even the standard version of the experiment. This increase is attributed to the larger effective area (see Fig. 5), which counterbalances the improvements in angular resolution.

B. Sensitivities

The number of gamma-ray events from ALPs emitted in BNS merger events and converting in the magnetic fields can be estimated as

$$N_{\text{ev}} = \int_{E_{\text{min}}}^{E_{\text{max}}} dE \frac{d\phi_{\gamma}}{dE} A_{\text{eff}}(E), \quad (21)$$

where $d\phi_{\gamma}/dE$ is the flux of photons reaching the Earth [see Eq. (18)]. The sensitivities to the ALP-photon coupling for the considered experiments are obtained by requiring that the number of ALP-induced gamma-ray events, N_{ev} , exceeds the number of background events, $N_{\text{ev}} \gtrsim N_{\text{bkg}}$ [see Eq. (19)].

Table II shows the sensitivities of the six experiments in the massless ALP limit ($m_a \lesssim 10^{-10} \text{eV}$) for a signal coming from a source located at $d = 4, 40, 100 \text{Mpc}$ in the same direction as the GW170817 event. We recall that, on average, choosing another sky location would affect the conversion probability by a factor of approximately a few (see Sec. IV B). Nevertheless, since the photon fluxes scale as $\sim g_{a\gamma}^4$, our limits on the ALP-photon coupling go as $\sim P_{a\gamma}^{1/4}$. Thus, our limits are expected to show a weak dependence on the sky location of the given event. Here $g_{a\pi}$ and $g_{a\gamma}$ are correlated as in Eq. (11). We find that the best sensitivity is achieved by MAST, which probes $g_{a\gamma} \gtrsim 0.27 \times 10^{-12} \text{GeV}^{-1}$ for $d = 40 \text{Mpc}$, while at that distance the other experiments have similar sensitivities, $g_{a\gamma} \gtrsim 10^{-12} \text{GeV}^{-1}$.

Experiment	Sensitivity on $g_{a\gamma} [\times 10^{-12} \text{ GeV}^{-1}]$		
	$d = 4 \text{ Mpc}$	$d = 40 \text{ Mpc}$	$d = 100 \text{ Mpc}$
e-ASTROGRAM [88]	0.3	1.1	1.7
AMEGO-X [89]	0.6	2.0	3.2
<i>Fermi</i> -LAT [90]	0.3	1.1	1.7
GRAMS-balloon [91]	0.4	1.4	2.2
GRAMS-satellite [91]	0.3	1.0	1.6
MAST [92]	0.08	0.27	0.4

TABLE II. Sensitivities of e-ASTROGRAM [88], AMEGO-X [89], *Fermi*-LAT [90], GRAMS-balloon [91], GRAMS-satellite [91], and MAST [92] in the massless ALP limit for a signal coming from a source located at $d = 4, 40, 100 \text{ Mpc}$ in the same direction as the GW170817 event, assuming $g_{a\gamma}$ and g_{ap} related as in Eq. (11).

In Fig. 6, we show the sensitivities associated with the different experiments in the plane $g_{a\gamma}$ vs m_a for a BNS system at the same sky location as the GW170817 event at $d = 4 \text{ Mpc}$ (upper panel), $d = 40 \text{ Mpc}$ (middle panel), and $d = 100 \text{ Mpc}$ (lower panel). Just like we did in Tab. II, also here we also assume that g_{ap} and $g_{a\gamma}$ are correlated as in Eq. (11). The shapes of these sensitivity curves exhibit a plateau in $g_{a\gamma}$ for $m_a \lesssim 10^{-9} \text{ eV}$ that corresponds to coherent ALP-photon conversions in the magnetic field of the Milky Way. For larger masses, the sensitivity deteriorates, until conversions in the magnetic field of the BNS mergers become dominant in the mass range $10^{-8} \text{ eV} \lesssim m_a \lesssim 10^{-3} \text{ eV}$, producing another plateau. For higher values of m_a , the conversions in the remnant are also strongly suppressed, producing a strong worsening in the sensitivity on $g_{a\gamma}$ (see Fig. 4).

The green region in Fig. 6 is excluded by astrophysical constraints [35, 95–98]. For comparison, we also show the most recent CAST bound from solar ALPs (dashed black curve) [99]. For the sake of clarity, we highlight that these constraints are placed by considering ALPs coupling to photons only. We also depict in yellow the band where preferred QCD axion models live (see, e.g., Ref. [14]). We remark that the BNS sensitivities as the other represented bounds (except the CAST one at higher masses) are very far to touch QCD axion models. An exception is the case of an ALP signal from a very nearby BNS merger at $d = 4 \text{ Mpc}$, where the sensitivity of the MAST experiment would touch the QCD axion band for $m_a \sim 10^{-3} \text{ eV}$. Furthermore, we show in light blue the bound from SN 1987A based on an excessive shortening of the observed neutrino burst, in the presence of a copious ALP emission by nuclear processes [21]. In order to have a direct comparison with a similar physics case, we also update the long-standing bound from the non-observation of a gamma-ray signal in coincidence with SN 1987A [32, 33], taking into account as the initial ALP spectrum the one shown in Fig. 3. Furthermore, we characterize ALP-photon conversions in the magnetic field of the SN, following the same model of Ref. [35], while for conversions in the Milky Way we refer to Sec. IV B. We remark that the conversions in the SN magnetic field produce a plateau in the exclusion plot in the mass range $10^{-8} \text{ eV} \lesssim m_a \lesssim 10^{-4} \text{ eV}$, due to an enhancement in the conversions for higher ALP masses, associated with the strong B -field in the source. Notice that the factor ~ 2 difference with respect to the results of Ref. [35] has to be attributed to different models of SN and Galactic magnetic fields, as well as the analysis methodologies adopted in the two works. We realize that, due to the lower emissivity of ALPs from BNS mergers, the SN 1987A bound is always stronger than possible sensitivities from BNS mergers, except for the case of the MAST experiment. Indeed, due to an extremely small background, MAST can probe ALP-photon couplings comparable to the SN 1987A one for ALP masses $m_a \lesssim 10^{-9} \text{ eV}$ and $d = 40 \text{ Mpc}$, and even better in the best-case scenario of $d = 4 \text{ Mpc}$.

C. Probability of joint GW-gamma detection

Finally, a key aspect to clarify is the typical rate at which a gamma-ray signal from extragalactic BNS mergers might be expected. This rate depends on the probability of observing an extra-galactic ALP-induced gamma-ray burst simultaneously with GW detection. Therefore, first one should evaluate the rate at which GWs from BNS systems can be observed by GW detectors. The authors of Ref. [100] proposed using the B -luminosity, i.e., the luminosity in the blue band, as a good tracer of recent star formation in the Universe. Therefore, starting with the estimated rate of BNS mergers in the Milky Way, one can extrapolate it to extra-galactic distances, rescaling it through the ratio of

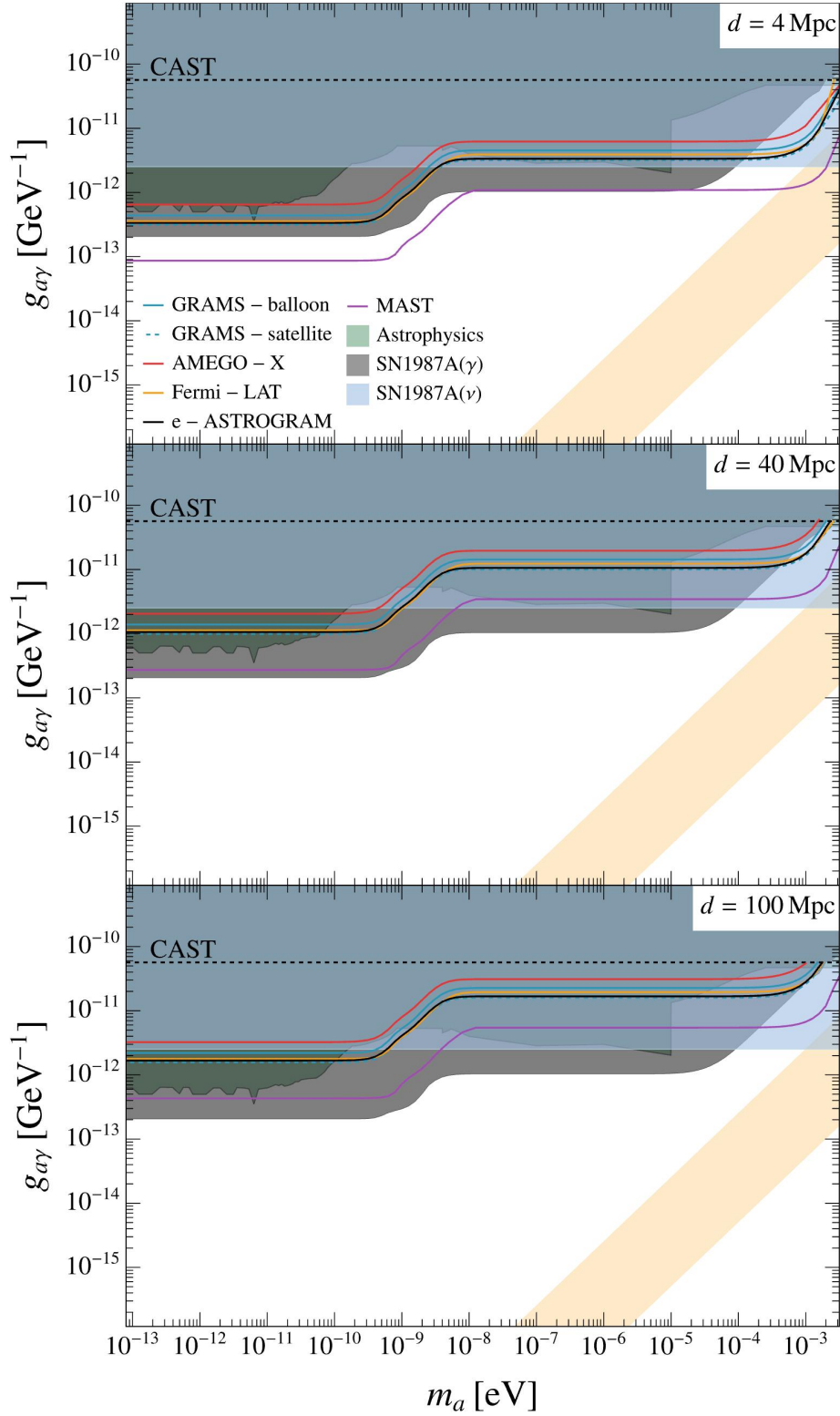


FIG. 6. Sensitivities of e-ASTROGRAM [88], AMEGO-X [89], *Fermi*-LAT [90], GRAMS-balloon [91], GRAMS-satellite [91], and MAST [92] in the plane $g_{a\gamma}$ vs m_a assuming that $g_{a\gamma}$ and $g_{a\gamma}$ are related as in Eq. (11). We assume a BNS system at the same sky location as the GW170817 event, at a distance of $d = 4$ Mpc (upper panel), $d = 40$ Mpc (middle panel), and $d = 100$ Mpc (lower panel) from the observer, respectively. The gray bound represents the limit for SN 1987A derived using the spectra shown in Fig. 3 and taking into account the conversion probability in the progenitor and the Milky Way magnetic fields [32, 33], and the dashed line shows the most recent CAST bound from solar axions [99]. Finally, the bounds in green correspond to constraints from other astrophysical observations [95–98]. We highlight that bounds in green are derived by assuming ALPs coupled to photons only.

Experiment	P_{on}	P_{FoV}	P_{tot}
<i>Fermi</i> -LAT, e-ASTROGRAM, AMEGO-X, MAST	85%	19%	16%
GRAMS-balloon, GRAMS-satellite	85%	50%	43%

TABLE III. Total probabilities P_{tot} to observe the portion of the sky in which the BNS event occurs for e-ASTROGRAM [88], AMEGO-X [89], *Fermi*-LAT [90], GRAMS-balloon [91], GRAMS-satellite [91], and MAST [92]. In particular, P_{on} represents the probability of the experiment being switched on during the occurrence of the BNS event and P_{FoV} denotes the probability of the event lying within the experiment FoV. With these definitions, $P_{\text{tot}} = P_{\text{on}} \times P_{\text{FoV}}$.

Experiment	T_{joint}		
	$d = 4 \text{ Mpc}$	$d = 40 \text{ Mpc}$	$d = 100 \text{ Mpc}$
<i>Fermi</i> -LAT, e-ASTROGRAM, AMEGO-X, MAST	$\sim (3-8) \times 10^5 \text{ yr}$	$\sim (3-8) \times 10^2 \text{ yr}$	$\sim 20-50 \text{ yr}$
GRAMS-balloon, GRAMS-satellite	$\sim (1-3) \times 10^5 \text{ yr}$	$\sim (1-3) \times 10^2 \text{ yr}$	$\sim 8-20 \text{ yr}$

TABLE IV. Average time interval T_{joint} between two joint GW-gamma detection by employing Advanced LIGO together with e-ASTROGRAM [88], AMEGO-X [89], *Fermi*-LAT [90], GRAMS-balloon [91], GRAMS-satellite [91], and MAST [92] for a BNS merger event located at $d = 4, 40, 100 \text{ Mpc}$.

B -luminosity at a certain distance d with respect to that in the Galaxy L_{MW} . Specifically, one gets [100]

$$\mathcal{R}_{\text{GW}} = \mathcal{R}_{\text{MW}} \left(\frac{L_{\text{total}}(d)}{L_{\text{MW}}} \right), \quad (22)$$

where the BNS merger rate in the Milky Way is given by

$$\mathcal{R}_{\text{MW}} = 42_{-14}^{+30} \text{ Myr}^{-1}, \quad (23)$$

as inferred from the Galactic pulsar population.

Choosing 100 Mpc as the GW detector horizon, as in the case of Advanced LIGO [101], the resulting GW detection rate would be given by [100]

$$R_{\text{GW}} \sim 0.18_{-0.06}^{+0.13} \times \left(\frac{d}{100 \text{ Mpc}} \right)^3 \text{ yr}^{-1}. \quad (24)$$

Thus, Advanced LIGO is expected to detect a BNS merger event at 100 Mpc from Earth approximately once every 3–8 years. We note, however, that for the next observing run starting in a few years, a detection horizon of 200 Mpc is anticipated, which would enhance the detection rate by approximately an order of magnitude.

Based on the above estimate [Eq. (24)], one can evaluate the probability of a joint gamma-GW signal detection. The gamma-ray detection probability P_{tot} is determined by the product of two factors, namely, the probability of the gamma-ray experiment being active during the occurrence of the BNS event (P_{on}), times the probability of the event falling within the experiment FoV (P_{FoV}). For all of the experiments, the first contribution is evaluated by assuming a survey mode similar to that of *Fermi*-LAT, i.e., $P_{\text{on}} = 85\%$, which accounts for the turning off of the instrument when passing through the South Atlantic Anomaly [102]. Moreover, by assuming isotropic distribution mergers, the probability of getting a BNS merger event in the experiment FoV is given by $P_{\text{FoV}} = \text{FoV}/4\pi$. We remark that, in the case of MAST, in the absence of detailed information, the FoV is assumed to be the same as that of *Fermi*-LAT. These probabilities computed for each of the considered experiments are shown in Tab. III. Finally, one can estimate the time interval between two joint-detection events by Advanced LIGO and gamma-ray experiments as

$$T_{\text{joint}} \simeq (R_{\text{GW}} \times P_{\text{on}} \times P_{\text{FoV}})^{-1}. \quad (25)$$

We show the computed values of T_{joint} for the different considered experiments in Tab. IV, where the given range is attributed to the uncertainty related to the GW detection rate. From Tab. IV we can see that for a source at a distance $d = 4 \text{ Mpc}$, the expected time to observe a BNS merger event is $\sim 10^5$ years, making this event extremely unlikely. Also the probability to get a joint detection at $d = 40 \text{ Mpc}$, i.e., the same distance as GW170817, is less than one per century. For sources at a distance of 100 Mpc, GRAMS-balloon and GRAMS-satellite are expected to achieve a joint detection of a BNS merger event approximately every 8–20 years. In contrast, the other experiments

are expected to achieve joint detections roughly once every 20–50 years. These results highlight the importance of achieving wider sky coverage [35]. If one assumes the employment of three experiments (for instance, AMEGO-X, *Fermi*-LAT, and GRAMS-satellite) in orbit at different points of the sky at the same time, it would be possible to cover up to 88% of the sky. Moreover, the probability of operational downtime could be considered negligible, as at least two out of the three experiments would remain operational. Under such conditions, the joint detection of a BNS event at 100 Mpc would be reduced to approximately once every 4–9 years.

Finally, we remark that a significant improvement in our analysis would be achieved thanks to the third-generation GW detectors, like the Einstein Telescope [103] or Cosmic Explorer detector [104], which could be operating in the mid 2030s with an improvement of one order of magnitude in GW sensitivities from BNS mergers with respect to detectors like Advanced LIGO. It has been estimated that such detectors can collect GW signals a few days before the neutron stars merge, for a distance $d \lesssim 200$ Mpc. This opportunity would be useful to get a localization and early warning of a BNS merger event, which could be exploited to allow the gamma-ray detectors to point in advance at the BNS merger and search for the ALP-induced gamma-ray burst. With this exciting possibility, one would expect to collect at least a BNS merger per decade in the relevant horizon for ALP searches.

VI. CONCLUSIONS

In this work, we have considered the physics potential of a multi-messenger detection of a gamma-ray burst induced by ALPs produced in extra-galactic BNS merger events, and then converting into photons in the remnant and Galactic magnetic field. We used as an external trigger for such an event the detection of the associated GW signal. We have shown that, assuming ALPs coupled to both nucleons and photons as in a canonical KSVZ model, current and planned gamma-ray telescopes operative in the MeV region can reach a sensitivity to the ALP-photon coupling down to $g_{a\gamma} \gtrsim \text{few} \times 10^{-13} \text{ GeV}^{-1}$ for $m_a \lesssim 10^{-9} \text{ eV}$, comparable with the SN 1987A limit. We remark that our analysis relies on conservative assumptions, such as spherical averaging over hydrodynamical quantities and ALPs coupling with only protons, which may underestimate the ALP flux and thus the predicted sensitivities. Furthermore, we have shown that in the most optimistic situation one can hope for a joint GW-gamma-ray signal every 5-10 years in a radius of 100 Mpc. Therefore, given sufficient time, one can accumulate statistics, improving the expected sensitivity through a stacked analysis.

In conclusion, our work shows that multi-messenger BNS merger detection could be exploited to search for ALPs, combining the unprecedented sensitivity of GW interferometers and gamma-ray detectors, to catch signals from merging neutron stars in the farthest regions of the Universe.

ACKNOWLEDGMENTS

We warmly thank Damiano Fiorillo and Edoardo Vitagliano for useful comments on the manuscript. We thank Tobias Fischer for useful discussions and providing analysis scripts. This article is based on work from COST Action COSMIC WISPerS CA21106, supported by COST (European Cooperation in Science and Technology). The work of AM and AL and FL was partially supported by the research grant number 2022E2J4RK "PANTHEON: Perspectives in Astroparticle and Neutrino THEory with Old and New messengers" under the program PRIN 2022 (Mission 4, Component 1, CUP I53D23001110006) funded by the Italian Ministero dell'Università e della Ricerca (MUR) and by the European Union – Next Generation EU. GL acknowledges support from the U.S. Department of Energy under contract number DE-AC02-76SF00515. This work is (partially) supported by ICSC – Centro Nazionale di Ricerca in High Performance Computing. VV and AB acknowledge support by the European Union through ERC Synergy Grant HeavyMetal no. 101071865. AB acknowledges support by the Deutsche Forschungsgemeinschaft (DFG, German Research Foundation) through Project - ID 279384907 – SFB 1245 (subprojects B07). MG acknowledges support from the Spanish Agencia Estatal de Investigación under grant PID2019-108122GB-C31, funded by MCIN/AEI/10.13039/501100011033, and from the "European Union NextGenerationEU/PRTR" (Planes complementarios, Programa de Astrofísica y Física de Altas Energías). He also acknowledges support from grant PGC2022-126078NB-C21, "Aún más allá de los modelos estándar," funded by MCIN/AEI/10.13039/501100011033 and "ERDF A way of making Europe." Additionally, MG acknowledges funding from the European Union's Horizon 2020 research and innovation programme under the European Research Council (ERC) grant agreement ERC-2017-AdG788781

(IAXO+).

-
- [1] J. Jaeckel and A. Ringwald, *The Low-Energy Frontier of Particle Physics*, *Ann. Rev. Nucl. Part. Sci.* **60** (2010) 405 [[1002.0329](#)].
 - [2] A. Ringwald, *Axions and Axion-Like Particles*, in *49th Rencontres de Moriond on Electroweak Interactions and Unified Theories*, pp. 223–230, 2014, [1407.0546](#).
 - [3] L. Di Luzio, M. Giannotti, E. Nardi and L. Visinelli, *The landscape of QCD axion models*, *Phys. Rept.* **870** (2020) 1 [[2003.01100](#)].
 - [4] P. Agrawal et al., *Feebly-interacting particles: FIPs 2020 workshop report*, *Eur. Phys. J. C* **81** (2021) 1015 [[2102.12143](#)].
 - [5] M. Giannotti, *Aspects of Axions and ALPs Phenomenology*, *J. Phys. Conf. Ser.* **2502** (2023) 012003 [[2205.06831](#)].
 - [6] C. Antel et al., *Feebly-interacting particles: FIPs 2022 Workshop Report*, *Eur. Phys. J. C* **83** (2023) 1122 [[2305.01715](#)].
 - [7] R. D. Peccei and H. R. Quinn, *CP Conservation in the Presence of Instantons*, *Phys. Rev. Lett.* **38** (1977) 1440.
 - [8] R. D. Peccei and H. R. Quinn, *Constraints Imposed by CP Conservation in the Presence of Instantons*, *Phys. Rev. D* **16** (1977) 1791.
 - [9] S. Weinberg, *A New Light Boson?*, *Phys. Rev. Lett.* **40** (1978) 223.
 - [10] F. Wilczek, *Problem of Strong P and T Invariance in the Presence of Instantons*, *Phys. Rev. Lett.* **40** (1978) 279.
 - [11] A. Arvanitaki, S. Dimopoulos, S. Dubovsky, N. Kaloper and J. March-Russell, *String Axiverse*, *Phys. Rev. D* **81** (2010) 123530 [[0905.4720](#)].
 - [12] M. Cicoli, M. Goodsell and A. Ringwald, *The type IIB string axiverse and its low-energy phenomenology*, *JHEP* **10** (2012) 146 [[1206.0819](#)].
 - [13] M. Cicoli, J. P. Conlon, A. Maharana, S. Parameswaran, F. Quevedo and I. Zavala, *String cosmology: From the early universe to today*, *Phys. Rept.* **1059** (2024) 1 [[2303.04819](#)].
 - [14] P. Carenza, M. Giannotti, J. Isern, A. Mirizzi and O. Straniero, *Axion Astrophysics*, [2411.02492](#).
 - [15] M. Carena and R. D. Peccei, *The Effective Lagrangian for Axion Emission From SN1987A*, *Phys. Rev. D* **40** (1989) 652.
 - [16] R. P. Brinkmann and M. S. Turner, *Numerical Rates for Nucleon-Nucleon Axion Bremsstrahlung*, *Phys. Rev. D* **38** (1988) 2338.
 - [17] G. Raffelt and D. Seckel, *A selfconsistent approach to neutral current processes in supernova cores*, *Phys. Rev. D* **52** (1995) 1780 [[astro-ph/9312019](#)].
 - [18] G. G. Raffelt, *Stars as laboratories for fundamental physics: The astrophysics of neutrinos, axions, and other weakly interacting particles*. 5, 1996.
 - [19] P. Carenza, T. Fischer, M. Giannotti, G. Guo, G. Martínez-Pinedo and A. Mirizzi, *Improved axion emissivity from a supernova via nucleon-nucleon bremsstrahlung*, *JCAP* **10** (2019) 016 [[1906.11844](#)]. [Erratum: JCAP 05, E01 (2020)].
 - [20] A. Lella, P. Carenza, G. Lucente, M. Giannotti and A. Mirizzi, *Protoneutron stars as cosmic factories for massive axionlike particles*, *Phys. Rev. D* **107** (2023) 103017 [[2211.13760](#)].
 - [21] A. Lella, P. Carenza, G. Co', G. Lucente, M. Giannotti, A. Mirizzi and T. Rauscher, *Getting the most on supernova axions*, *Phys. Rev. D* **109** (2024) 023001 [[2306.01048](#)].
 - [22] P. Carenza, B. Fore, M. Giannotti, A. Mirizzi and S. Reddy, *Enhanced Supernova Axion Emission and its Implications*, *Phys. Rev. Lett.* **126** (2021) 071102 [[2010.02943](#)].
 - [23] G. G. Raffelt and D. S. P. Dearborn, *Bounds on Hadronic Axions From Stellar Evolution*, *Phys. Rev. D* **36** (1987) 2211.
 - [24] G. Raffelt and L. Stodolsky, *Mixing of the Photon with Low Mass Particles*, *Phys. Rev. D* **37** (1988) 1237.
 - [25] KAMIOKANDE-II Collaboration, K. Hirata et al., *Observation of a Neutrino Burst from the Supernova SN 1987a*, *Phys. Rev. Lett.* **58** (1987) 1490.
 - [26] K. S. Hirata et al., *Observation in the Kamiokande-II Detector of the Neutrino Burst from Supernova SN 1987a*, *Phys. Rev. D* **38** (1988) 448.
 - [27] R. M. Bionta et al., *Observation of a Neutrino Burst in Coincidence with Supernova SN 1987a in the Large Magellanic Cloud*, *Phys. Rev. Lett.* **58** (1987) 1494.
 - [28] IMB Collaboration, C. B. Bratton et al., *Angular Distribution of Events From Sn1987a*, *Phys. Rev. D* **37** (1988) 3361.
 - [29] E. N. Alekseev, L. N. Alekseeva, I. V. Krivosheina and V. I. Volchenko, *Detection of the Neutrino Signal From SN1987A in the LMC Using the Inr Baksan Underground Scintillation Telescope*, *Phys. Lett. B* **205** (1988) 209.
 - [30] J. A. Grifols, E. Masso and R. Toldra, *Gamma-rays from SN1987A due to pseudoscalar conversion*, *Phys. Rev. Lett.* **77** (1996) 2372 [[astro-ph/9606028](#)].
 - [31] J. W. Brockway, E. D. Carlson and G. G. Raffelt, *SN1987A gamma-ray limits on the conversion of pseudoscalars*, *Phys. Lett. B* **383** (1996) 439 [[astro-ph/9605197](#)].
 - [32] A. Payez, C. Evoli, T. Fischer, M. Giannotti, A. Mirizzi and A. Ringwald, *Revisiting the SN1987A gamma-ray limit on ultralight axion-like particles*, *JCAP* **02** (2015) 006 [[1410.3747](#)].
 - [33] S. Hoof and L. Schulz, *Updated constraints on axion-like particles from temporal information in supernova SN1987A gamma-ray data*, *JCAP* **03** (2023) 054 [[2212.09764](#)].
 - [34] F. Calore, P. Carenza, M. Giannotti, J. Jaeckel and A. Mirizzi, *Bounds on axionlike particles from the diffuse supernova flux*, *Phys. Rev. D* **102** (2020) 123005 [[2008.11741](#)].

- [35] C. A. Manzari, Y. Park, B. R. Safdi and I. Savoray, *Supernova Axions Convert to Gamma Rays in Magnetic Fields of Progenitor Stars*, *Phys. Rev. Lett.* **133** (2024) 211002 [2405.19393].
- [36] T. Dietrich and K. Clough, *Cooling binary neutron star remnants via nucleon-nucleon-axion bremsstrahlung*, *Phys. Rev. D* **100** (2019) 083005 [1909.01278].
- [37] D. F. G. Fiorillo and F. Iocco, *Axions from neutron star mergers*, *Phys. Rev. D* **105** (2022) 123007.
- [38] LIGO SCIENTIFIC Collaboration, G. M. Harry, *Advanced LIGO: The next generation of gravitational wave detectors*, *Class. Quant. Grav.* **27** (2010) 084006.
- [39] VIRGO Collaboration, F. Acernese et al., *Advanced Virgo: a second-generation interferometric gravitational wave detector*, *Class. Quant. Grav.* **32** (2015) 024001 [1408.3978].
- [40] LIGO SCIENTIFIC, VIRGO, FERMI GBM, INTEGRAL, IceCUBE, ASTROSat CADMIUM ZINC TELLURIDE IMAGER TEAM, IPN, INSIGHT-HXMT, ANTARES, SWIFT, AGILE TEAM, 1M2H TEAM, DARK ENERGY CAMERA GW-EM, DES, DLT40, GRAWITA, FERMI-LAT, ATCA, ASKAP, LAS CUMBRES OBSERVATORY GROUP, OzGRAV, DWF (DEEPER WIDER FASTER PROGRAM), AST3, CAASTRO, VINROUGE, MASTER, J-GEM, GROWTH, JAGWAR, CALTECHNRAO, TTU-NRAO, NuSTAR, PAN-STARRS, MAXI TEAM, TZAC CONSORTIUM, KU, NORDIC OPTICAL TELESCOPE, EPESSTO, GROND, TEXAS TECH UNIVERSITY, SALT GROUP, TOROS, BOOTES, MWA, CALET, IKI-GW FOLLOW-UP, H.E.S.S., LOFAR, LWA, HAWC, PIERRE AUGER, ALMA, EURO VLBI TEAM, PI OF SKY, CHANDRA TEAM AT MCGILL UNIVERSITY, DFN, ATLAS TELESCOPES, HIGH TIME RESOLUTION UNIVERSE SURVEY, RIMAS, RATIR, SKA SOUTH AFRICA/MEERKAT Collaboration, B. P. Abbott et al., *Multi-messenger Observations of a Binary Neutron Star Merger*, *Astrophys. J. Lett.* **848** (2017) L12 [1710.05833].
- [41] FERMI-LAT Collaboration, D. Kocevski, N. Omodei and G. Vianello, *Fermi-LAT observations of the LIGO/Virgo event GW170817*, **1710.05450**.
- [42] LIGO SCIENTIFIC, VIRGO, FERMI-GBM, INTEGRAL Collaboration, B. P. Abbott et al., *Gravitational Waves and Gamma-rays from a Binary Neutron Star Merger: GW170817 and GRB 170817A*, *Astrophys. J. Lett.* **848** (2017) L13 [1710.05834].
- [43] V. Savchenko et al., *INTEGRAL Detection of the First Prompt Gamma-Ray Signal Coincident with the Gravitational-wave Event GW170817*, *Astrophys. J. Lett.* **848** (2017) L15 [1710.05449].
- [44] L. Baiotti and L. Rezzolla, *Binary neutron star mergers: a review of Einstein's richest laboratory*, *Rept. Prog. Phys.* **80** (2017) 096901 [1607.03540].
- [45] S. Typel, G. Röpke, T. Klähn, D. Blaschke and H. H. Wolter, *Composition and thermodynamics of nuclear matter with light clusters*, *Phys. Rev. C* **81** (2010) 015803.
- [46] R. Ardevol-Pulpillo, H. T. Janka, O. Just and A. Bauswein, *Improved leakage-equilibration-absorption scheme (ILEAS) for neutrino physics in compact object mergers*, **1808.00006**.
- [47] C. E. Collins, A. Bauswein, S. A. Sim, V. Vijayan, G. Martínez-Pinedo, O. Just, L. J. Shingles and M. Kromer, *3D radiative transfer kilonova modelling for binary neutron star merger simulations*, *Mon. Not. R. Astron. Soc.* **521** (2023) 1858.
- [48] N. Iwamoto, *Axion Emission from Neutron Stars*, *Phys. Rev. Lett.* **53** (1984) 1198.
- [49] M. Hempel, *Nucleon self-energies for supernova equations of state*, *Phys. Rev. C* **91** (2015) 055807 [1410.6337].
- [50] G. Martínez-Pinedo, T. Fischer, A. Lohs and L. Huther, *Charged-current weak interaction processes in hot and dense matter and its impact on the spectra of neutrinos emitted from proto-neutron star cooling*, *Phys. Rev. Lett.* **109** (2012) 251104 [1205.2793].
- [51] W. Keil, H.-T. Janka, D. N. Schramm, G. Sigl, M. S. Turner and J. R. Ellis, *A Fresh look at axions and SN-1987A*, *Phys. Rev. D* **56** (1997) 2419 [astro-ph/9612222].
- [52] K. Springmann, M. Stadlbauer, S. Stelzl and A. Weiler, *From supernovae to neutron stars: a systematic approach to axion production at finite density*, *JHEP* **02** (2025) 138 [2410.10945].
- [53] V. Vijayan, N. Rahman, A. Bauswein, G. Martínez-Pinedo and I. L. Arbina, *Impact of pions on binary neutron star mergers*, *Phys. Rev. D* **108** (2023) 023020 [2302.12055].
- [54] M. A. Pajkos and E. R. Most, *Influence of muons, pions, and trapped neutrinos on neutron star mergers*, *Phys. Rev. D* **111** (2025) 043013 [2409.09147].
- [55] F. Calore, P. Carenza, C. Eckner, T. Fischer, M. Giannotti, J. Jaeckel, K. Kotake, T. Kuroda, A. Mirizzi and F. Sivo, *3D template-based Fermi-LAT constraints on the diffuse supernova axion-like particle background*, *Phys. Rev. D* **105** (2022) 063028 [2110.03679].
- [56] P. S. B. Dev, J.-F. Fortin, S. P. Harris, K. Sinha and Y. Zhang, *First Constraints on the Photon Coupling of Axionlike Particles from Multimessenger Studies of the Neutron Star Merger GW170817*, *Phys. Rev. Lett.* **132** (2024) 101003 [2305.01002].
- [57] M. Diamond, D. F. G. Fiorillo, G. Marques-Tavares, I. Tamborra and E. Vitagliano, *Multimessenger Constraints on Radiatively Decaying Axions from GW170817*, *Phys. Rev. Lett.* **132** (2024) 101004 [2305.10327].
- [58] H. Kochankovski, G. Lioutas, S. Blacker, A. Bauswein, A. Ramos and L. Tolos, *The impact of hyperons on neutron star mergers: gravitational waves, mass ejection and black hole formation*, *arXiv e-prints* (2025) arXiv:2501.12905 [2501.12905].
- [59] J. E. Kim, *Weak Interaction Singlet and Strong CP Invariance*, *Phys. Rev. Lett.* **43** (1979) 103.
- [60] M. A. Shifman, A. Vainshtein and V. I. Zakharov, *Can Confinement Ensure Natural CP Invariance of Strong Interactions?*, *Nucl. Phys. B* **166** (1980) 493.
- [61] G. Grilli di Cortona, E. Hardy, J. Pardo Vega and G. Villadoro, *The QCD axion, precisely*, *JHEP* **01** (2016) 034 [1511.02867].

- [62] S. P. Harris, J.-F. Fortin, K. Sinha and M. G. Alford, *Axions in neutron star mergers*, *JCAP* **07** (2020) 023 [2003.09768].
- [63] V. Paschalidis, *General relativistic simulations of compact binary mergers as engines for short gamma-ray bursts*, *Class. Quant. Grav.* **34** (2017) 084002 [1611.01519].
- [64] M. D. Duez and Y. Zlochower, *Numerical Relativity of Compact Binaries in the 21st Century*, *Rept. Prog. Phys.* **82** (2019) 016902 [1808.06011].
- [65] R. Cioffi, *The key role of magnetic fields in binary neutron star mergers*, *Gen. Rel. Grav.* **52** (2020) 59 [2003.07572].
- [66] J.-F. Fortin and K. Sinha, *Constraining Axion-Like-Particles with Hard X-ray Emission from Magnetars*, *JHEP* **06** (2018) 048 [1804.01992].
- [67] C. Dessert, A. J. Long and B. R. Safdi, *X-ray Signatures of Axion Conversion in Magnetic White Dwarf Stars*, *Phys. Rev. Lett.* **123** (2019) 061104 [1903.05088].
- [68] W. Heisenberg and H. Euler, *Consequences of Dirac's theory of positrons*, *Z. Phys.* **98** (1936) 714 [physics/0605038].
- [69] R. Jansson and G. R. Farrar, *A New Model of the Galactic Magnetic Field*, *Astrophys. J.* **757** (2012) 14 [1204.3662].
- [70] A. Fletcher, *Magnetic fields in nearby galaxies*, *ASP Conf. Ser.* **438** (2011) 197 [1104.2427].
- [71] R. Beck and R. Wielebinski, *Magnetic Fields in the Milky Way and in Galaxies*. 2, 2013. 1302.5663. 10.1007/978-94-007-5612-0_13.
- [72] R. Pakmor, F. A. Gómez, R. J. J. Grand, F. Marinacci, C. M. Simpson, V. Springel, D. J. R. Campbell, C. S. Frenk, T. Guillet, C. Pfrommer and S. D. M. White, *Magnetic field formation in the Milky Way like disc galaxies of the Auriga project*, *Monthly Notices of the Royal Astronomical Society* **469** (2017) 3185 [1701.07028].
- [73] A. Mirizzi and D. Montanino, *Stochastic conversions of TeV photons into axion-like particles in extragalactic magnetic fields*, *JCAP* **12** (2009) 004 [0911.0015].
- [74] A. Kartavtsev, G. Raffelt and H. Vogel, *Extragalactic photon-ALP conversion at CTA energies*, *JCAP* **01** (2017) 024 [1611.04526].
- [75] A. M. Taylor, I. Vovk and A. Neronov, *Extragalactic magnetic fields constraints from simultaneous GeV-TeV observations of blazars*, *Astron. Astrophys.* **529** (2011) A144 [1101.0932].
- [76] R. Durrer and A. Neronov, *Cosmological Magnetic Fields: Their Generation, Evolution and Observation*, *Astron. Astrophys. Rev.* **21** (2013) 62 [1303.7121].
- [77] C. Caprini and S. Gabici, *Gamma-ray observations of blazars and the intergalactic magnetic field spectrum*, *Phys. Rev. D* **91** (2015) 123514 [1504.00383].
- [78] M. S. Pshirkov, P. G. Tinyakov, P. P. Kronberg and K. J. Newton-McGee, *Deriving global structure of the Galactic Magnetic Field from Faraday Rotation Measures of extragalactic sources*, *Astrophys. J.* **738** (2011) 192 [1103.0814].
- [79] M. Unger and G. R. Farrar, *The Coherent Magnetic Field of the Milky Way*, *Astrophys. J.* **970** (2024) 95 [2311.12120].
- [80] B. Gold et al., *Seven-Year Wilkinson Microwave Anisotropy Probe (WMAP) Observations: Galactic Foreground Emission*, *Astrophys. J. Suppl.* **192** (2011) 15 [1001.4555].
- [81] PLANCK Collaboration, R. Adam et al., *Planck intermediate results.: XLII. Large-scale Galactic magnetic fields*, *Astron. Astrophys.* **596** (2016) A103 [1601.00546].
- [82] PLANCK Collaboration, R. Adam et al., *Planck 2015 results. I. Overview of products and scientific results*, *Astron. Astrophys.* **594** (2016) A1 [1502.01582].
- [83] PLANCK Collaboration, P. A. R. Ade et al., *Planck 2015 results - II. Low Frequency Instrument data processings*, *Astron. Astrophys.* **594** (2016) A2 [1502.01583].
- [84] PLANCK Collaboration, P. A. R. Ade et al., *Planck 2015 results. VI. LFI mapmaking*, *Astron. Astrophys.* **594** (2016) A6 [1502.01585].
- [85] D. Horns, L. Maccione, M. Meyer, A. Mirizzi, D. Montanino and M. Roncadelli, *Hardening of TeV gamma spectrum of AGNs in galaxy clusters by conversions of photons into axion-like particles*, *Phys. Rev. D* **86** (2012) 075024 [1207.0776].
- [86] DES, DARK ENERGY CAMERA GW-EM Collaboration, M. Soares-Santos et al., *The Electromagnetic Counterpart of the Binary Neutron Star Merger LIGO/Virgo GW170817. I. Discovery of the Optical Counterpart Using the Dark Energy Camera*, *Astrophys. J. Lett.* **848** (2017) L16 [1710.05459].
- [87] F. Calore, P. Carenza, C. Eckner, M. Giannotti, G. Lucente, A. Mirizzi and F. Sivo, *Uncovering axionlike particles in supernova gamma-ray spectra*, *Phys. Rev. D* **109** (2024) 043010 [2306.03925].
- [88] e-ASTROGAM Collaboration, A. De Angelis et al., *The e-ASTROGAM mission*, *Exper. Astron.* **44** (2017) 25 [1611.02232].
- [89] R. Caputo et al., *All-sky Medium Energy Gamma-ray Observatory eXplorer mission concept*, *J. Astron. Telesc. Instrum. Syst.* **8** (2022) 044003 [2208.04990].
- [90] FERMI-LAT Collaboration, M. Ajello et al., *Fermi Large Area Telescope Performance after 10 Years of Operation*, *Astrophys. J. Suppl.* **256** (2021) 12 [2106.12203].
- [91] T. Aramaki, P. Hansson Adrian, G. Karagiorgi and H. Odaka, *Dual MeV Gamma-Ray and Dark Matter Observatory - GRAMS Project*, *Astropart. Phys.* **114** (2020) 107 [1901.03430].
- [92] T. Dzhatdov and E. Podlesnyi, *Massive Argon Space Telescope (MAST): A concept of heavy time projection chamber for γ -ray astronomy in the 100 MeV–1 TeV energy range*, *Astropart. Phys.* **112** (2019) 1 [1902.01491].
- [93] E. Müller, P. Carenza, C. Eckner and A. Goobar, *Constraining MeV-scale axionlike particles with Fermi-LAT observations of SN 2023jzf*, *Phys. Rev. D* **109** (2024) 023018 [2306.16397].
- [94] P. Carenza and P. De la Torre Luque, *Detecting neutrino-boosted axion dark matter in the MeV gap*, *Eur. Phys. J. C* **83** (2023) 110 [2210.17206].

- [95] FERMI-LAT Collaboration, M. Ajello et al., *Search for Spectral Irregularities due to Photon–Axionlike-Particle Oscillations with the Fermi Large Area Telescope*, *Phys. Rev. Lett.* **116** (2016) 161101 [[1603.06978](#)].
- [96] D. Noordhuis, A. Prabhu, S. J. Witte, A. Y. Chen, F. Cruz and C. Weniger, *Novel Constraints on Axions Produced in Pulsar Polar-Cap Cascades*, *Phys. Rev. Lett.* **131** (2023) 111004 [[2209.09917](#)].
- [97] H.-J. Li, W. Chao and Y.-F. Zhou, *Upper limit on the axion-photon coupling from Markarian 421*, *Phys. Lett. B* **858** (2024) 139075 [[2406.00387](#)].
- [98] O. Ning and B. R. Safdi, *Leading Axion-Photon Sensitivity with NuSTAR Observations of M82 and M87*, [2404.14476](#).
- [99] CAST Collaboration, K. Altenmüller et al., *New Upper Limit on the Axion-Photon Coupling with an Extended CAST Run with a Xe-Based Micromegas Detector*, *Phys. Rev. Lett.* **133** (2024) 221005 [[2406.16840](#)].
- [100] N. Pol, M. McLaughlin and D. R. Lorimer, *Future prospects for ground-based gravitational wave detectors – The Galactic double neutron star merger rate revisited*, *Astrophys. J.* **870** (2019) 71 [[1811.04086](#)]. [Erratum: *Astrophys. J.* **874**, 186 (2019)].
- [101] KAGRA, LIGO SCIENTIFIC, VIRGO Collaboration, B. P. Abbott et al., *Prospects for observing and localizing gravitational-wave transients with Advanced LIGO, Advanced Virgo and KAGRA*, *Living Rev. Rel.* **19** (2016) 1 [[1304.0670](#)].
- [102] FERMI-LAT Collaboration, R. Pilleri, *Science highlights of the Fermi-LAT*, *Nuovo Cim. C* **47** (2024) 73.
- [103] ET Collaboration, M. Maggiore et al., *Science Case for the Einstein Telescope*, *JCAP* **03** (2020) 050 [[1912.02622](#)].
- [104] M. Evans et al., *A Horizon Study for Cosmic Explorer: Science, Observatories, and Community*, [2109.09882](#).